Toxicology Research

PAPER

View Article Online
View Journal | View Issue

Cite this: *Toxicol. Res.*, 2018, **7**, 959

Molecular insight to size and dose-dependent cellular toxicity exhibited by a green synthesized bioceramic nanohybrid with macrophages for dental applications†

Hardik Makkar, ‡[a] Suresh K. Verma, ‡[b] Pritam Kumar Panda, [c] Nandini Pramanik,[d] Ealisha Jha[e] and Mrutyunjay Suar *[a,b]

Improvising bioceramics for enhancing their biocompatibility and physical properties has been a focus area for the dental industry. To further explore this area, this study reports a novel green synthesis and molecular *in vitro* biocompatibility of calcium aluminosilicate–chitosan nanohybrid (CAS–CH). The nanohybrids were synthesized by using a high energy ball milling (HEBM) technique and then characterized for their physiochemical properties using standard techniques including scanning electron microscopy (SEM) and dynamic light scattering (DLS). *In vitro* cytotoxicity evaluation of a synthesized nanohybrid was made with a RAW264.7 cell line using cell viability assays, such as, MTT, cellular morphology analysis, induction of oxidative stress, and apoptosis. CAS–CH nanohybrids were synthesized at three milling time points: 1H, 2H, and 3H. With increasing milling time, we found a reduction in sizes of particles and increased zeta potential. Viability of cells was found to be decreased with an increase in concentration. Moreover, toxic effects like ROS generation and apoptosis were reduced with increasing milling time. Computational and experimental analysis elucidated the mechanism of toxicity as a consequence of influential functionality of Sod1 and p53 proteins due to interaction and internalization of the nanohybrids with amino acid residues *via* hydrogen bonds and hydrophobic interactions. The detailed study depicted a novel way of synthesizing biocompatible bioceramic nanohybrids with a mechanistic insight of its cytotoxicity profile.

Received 14th April 2018,
Accepted 18th June 2018

DOI: 10.1039/c8tx00112j

rsc.li/toxicology-research

Introduction

Ceramics have a known reputation in last few decades for their utilities in day-to-day life. Their use far extends into significantly improving the quality of life. This can be attributed to their physical, chemical, and biological properties, made suitable to aid in repair, replacement, and regeneration of diseased or lost tissues.[1] With the gaining popularity of ceramics for biomedical applications, improvising their biocompatibility and bioactivity has been an area of focus for researchers and industry. This has led to the introduction of bioceramics which are significantly contributing to improving the health of patients owing to their wide applications as materials used for dental implants, treating bone defects and fractures, joint replacements, and craniomaxillary reconstruction.[2] Based on their uses and properties, bioceramics have been classified as: those with single crystals, polycrystalline,[3] and glass-based or composites.[4,5] The use of bioceramics specifically in dentistry has been a reality for the last ten years. They are available in the form of hydraulic cements (cements setting in the presence of water) used for root repair, pulp capping, root-end filling, root canal filling core, and sealer materials.[6] Their widespread use in dentistry is due to their biological apatite similar to dental hard tissues.[7,8]

The first commercially available bioceramic for dental application was a mineral trioxide aggregate which was derived from Portland cement[9] and was comprised of tri-calcium silicate, tri-calcium aluminate, bismuth oxide, and tri-calcium oxide.[10] This material was extensively evaluated for its strength properties and biocompatibility.[11] However, traditional bioceramics for dental applications also have been reported with disadvantages including long setting times, difficulty in

[a]*KIIT Technology Business incubator, KIIT University, Bhubaneswar, Orissa, 751024, India. E-mail: msuar@kiitbiotech.ac.in*
[b]*School of Biotechnology, KIIT University, Bhubaneswar, Orissa, 751024, India*
[c]*University of Freiburg, Division of Paediatric Haematology and Oncology, Freiburg, 79106, Germany*
[d]*Advance Science and Technology Research Centre, Vinoba Bhave University, Hazaribagh, Jharkhand, 825301, India*
[e]*Memorial University of Newfoundland, Department of Physics and Physical Oceanography, St John's, Newfoundland and Labrador, NL A1C 5S7 Canada*
†Electronic supplementary information (ESI) available. See DOI: 10.1039/c8tx00112j
‡These authors have contributed equally as first author.

manipulation, and cytotoxicity.[12,13] In the quest for solutions for these issues, hydraulic aluminate cement recently gained attention as being more durable than conventional Portland cement. This is ascribed to its compositional variation, where the hydraulic calcium phase has a high alumina content.[13] Moreover, they have a track record of being well known and superior bone cements due to their high strength properties when compared to alternatives like polymethyl methacrylate bone cements.[14] A critical, but less discussed issue related to clinical use of bioceramics, includes their contamination with blood and tissue fluids when placed at the surgical site. This leads to detrimental effects on material strength, microstructure, and bioactivity[15] due to their inability to induce hemostasis.

Hence, in view of the problems discussed above, it is the need of hour to synthesize new bioceramic materials having more durability, biocompatibility, and bioactivity. In order to develop such materials, there is a need for utilizing a technique which would allow blending of other biocompatible materials with bioceramics in order to overcome these issues and improve their biological qualities.

Chitosan, a partially de-acetylated derivative of chitin, has been popularly studied for biomedical applications[16] and shown to have inherent chondrogenic and osteogenic potential, antibacterial activity, ability to enhance wound healing, and to induce hemostasis.[17] This makes it a probable candidate to be investigated as a blending material with calcium aluminosilicate for dental applications.

The present study showcased fabrication of a calcium aluminosilicate–chitosan (CAS–CH) nano hybrid using a high energy ball milling (HEBM) technique. HEBM has been recognized as a green methodology for synthesis of nanomaterials.[18] A benefit of HEBM includes using mechanical energy, controlled synthesis, and eco-compatibility.[19] The synthesized material was characterized using Scanning Electron Microscopy (SEM) and Dynamic Light Scattering (DLS) for their physiochemical properties. The *in vitro* biocompatibility of this novel material was analyzed using MTT assay and its ability to induce oxidative stress and apoptosis in murine macrophages. An *in silico* approach was used to analyze the effective influence and interactions of the synthesized material with cellular metabolic proteins like Sod1 and p53. The study revealed chitosan as a promising blending material with calcium aluminosilicate for dental applications with its probable *in vitro* cytotoxicity profile.

Materials and methods

Synthesis of calcium aluminosilicate–chitosan nano hybrid

Synthesis of calcium aluminosilicate–chitosan nano hybrid was performed by using a high energy ball milling method (HEBM). Pre-sintered calcium aluminosilicate pellets with an average size of 4 mm × 1.5 mm × 2 mm and chitosan (75% deacetylated) were blended in a ratio of 5 : 1 using a ball milling machine (Retsch, PM250). The milling was done in a tungsten carbide container (250 mL) using 10 mm tungsten carbide balls under dry conditions and ambient temperature. The assembly revolved at 300 rpm with a ball to powder ratio maintained at 20 : 1. Dry milling was done for three hours and the samples were collected at 1 h (hour), 2 h, and 3 h. The prepared samples were termed: CAS–CH 1H, CAS–CH 2H, and CAS–CH 3H.

Physiochemical characterization of synthesized nanohybrid

The physiochemical characterization of synthesized CAS–CH 1H, CAS–CH 2H, and CAS–CH 3H was accomplished using standard techniques. Size was assessed using a scanning electron microscope (SEM) following which the particle size distribution in the images was analyzed using Image J. For SEM analysis, samples of CAS–CH 1H, CAS–CH 2H, and CAS–CH 3H were suspended in a water medium and then dried on the surface of a silicon chip before exposing it to the instrument (Carl Zeiss, Neon 40 microscope) at 20 kV. The hydrodynamic size of a nanohybrid in DMEM cell culture medium was determined using a dynamic light scattering technique by Zetasizer (Malvern, UK). The zeta potential of the samples immersed in cell culture media was evaluated for determination of sample stability by using a Zetasizer (Malvern, UK).

Preparation of samples for cellular assays

The sample preparation of CAS–CH 1H, CAS–CH 2H, and CAS–CH 3H for cytotoxicity assays was done in accordance with ISO 10993-12. Briefly, the test materials were mixed with distilled water (powder liquid ratio 2 : 1) and placed in sterile cylindrical molds (diameter 5 mm, height 4 mm). The filled molds were then incubated at 37° C with 5% CO_2 for 24 hours for complete setting of the materials. Samples were retrieved from the molds and sterilized by exposing them to UV radiation for 20 minutes. This was followed by their incubation with 15 mL of Dulbecco modified essential medium, supplemented with 10% fetal bovine serum, 100 units per mL penicillin, and 100 mg mL^{-1} streptomycin at 37° C with 5% CO2 for 24 hours to allow extraction of material constituents in the media (ratio of 0.5 cm^2 mL^{-1}). The supernatant (eluate extract) was collected and filtered through a 0.22 μm filter. The collected supernatant was referred to as bulk concentration extract (X) and was diluted twice (X/2) and four times (X/4) for each test group.

Cell culture

The *in vitro* cytotoxicity studies were performed with RAW 264.7 (ATCC® TIB71™). Supplied RAW 264.7, Passage 2 (0.5×10^6 cells per vial) cells was thawed at 37 °C in a water bath. The cell suspensions were sub-cultured in a T 25 flask. The cells were incubated 37 °C with 5% CO_2 for further attachment and passage.

Cell proliferation assay

Viability and proliferation of RAW 264.7 (ATCC® TIB71™) after exposure with CAS–CH 1H, CAS–CH 2H, and CAS–CH 3H at different concentrations (X, X/2, and X/4) were evaluated by

analyzing their morphological changes using bright field microscopy and by MTT Assay (Vybrant MTT cell proliferation assay kit, Molecular Probes, USA). The protocol was followed as instructed in the kit. In brief, cells were resuspended in a complete media and 10^4 cells per well were seeded in a 96 well plate. The cells were incubated for 16 h at 37 °C with 5% CO_2 for their proper attachment. After ensuring attachment of the cells, the media was replaced with test material extract at different concentrations and proliferation was analyzed after 48 hours. RAW 264.7 cells cultured in untreated media were taken as a control. Cells were imaged using bright-field microscope (Thermofisher Scientific, USA) and morphological changes were evaluated. Following treatment, the cells were washed twice with PBS and incubated with MTT dye (10 μL of the 12 mM MTT stock solution per well) for 4 hours. This was followed by adding 100 μL of the SDS-HCl solution and incubated at 37 °C for 4 hours in a humidified chamber. Absorbance was read at 570 nm by an automatic microplate reader (Epoch, ELISA plate reader). All samples were assessed in triplicate and analyzed statistically using Graph Pad Prism v6.1. Two way ANOVA was used to assess significance of difference between the groups.

Reactive oxygen species and apoptosis analysis

To understand the cellular mechanism of cytotoxicity of CAS–CH, ROS production and induction of apoptosis was analyzed using dihydroethidium (DHE) and acridine orange – ethidium bromide staining, respectively. Briefly, for ROS analysis, after 48 h of treatment with material extracts, cells were stained with DHE for 20 m in the dark. Following staining, the cells were analyzed and quantified for intracellular superoxide production using flow cytometry (Attune, Applied Biosystems, Life Technologies). The experiment was performed in triplicate and the data was analyzed with Facsxpress (Denovo, CA). Statistical analysis and test of significance was calculated using Graph Pad prism v6.1.

Acridine orange/ethidium bromide assay[20] was done to assess apoptosis in RAW 264.7 (ATCC® TIB71™) treated with extracts of CAS–CH nanohybrid. Apoptosis in the cells was analyzed at 48 hours. The test and control groups in each well were stained with 10 μL of acridine orange/ethidium bromide solution and observed under a fluorescent microscope (Evos, Thermo Scientific). Image analysis and assessment was done by determination of the mean fluorescence intensity using Image J. All samples were assessed in triplicate and analyzed statistically using Graph Pad Prism v6.1. Two way ANOVA was used to assess significance of difference between groups.

In silico molecular analysis

Molecular docking studies were used to determine interaction of the ligand and the protein to know the preferred binding orientations of a ligand that confers a minimum binding energy (generally in negative energies). The analysis was performed using Autodock 4.2 using calcium aluminosilicate & chitosan as ligand and Sod1, p53 as receptor protein. Chemical structures were retrieved from PubChem and visualized using Chimera and their geometries were optimized using a Gaussian 03 program.[21] The receptor proteins were subjected to energy minimization using the Chimera program.[22] Parameters for the chemical structures were set for Autodock 4.2.[23] Grid dimensions were set to 40 × 40 × 40, with a spacing of 1 Å. Lamarckian genetic algorithms (LGA) was used for grid dimensions. Genetic algorithm was used for docking runs using a population size of 150 with a maximum number of evaluations set to 2 500 000 and maximal generations. The post-docking analysis was performed using Autodock 4.2 analysis tools using conformations and clustering and visualized using Chimera.

Results

Synthesis and physicochemical properties of the CAS–CH nanohybrid

CAS–CH nanohybrid was synthesized by HEBM for 1H, 2H, and 3H as shown in Fig. 1. Synthesized materials were further evaluated for their physiochemical properties. As shown in Fig. 2, scanning electron micrographs show particles of various sizes and shapes ranging from 2.8 nm to 2.1 μm with a progressive decrease in the overall size of the CAS–CH nanohybrid from 1 h to 3 h. The particle size distributions in CAS–CH 1H, CAS–CH 2H, and CAS–CH 3H are presented in Table 1.

The average hydrodynamic size of the materials as assessed by the dynamic light scattering method was found to exhibit a similar result of a progressive decrease in size with an increase in milling time (Table 2). The CAS–CH 1H sample had a mean hydrodynamic particle size of 576.7 nm ± 111.1. CAS–CH 2H, and CAS–CH 3H sample had mean hydrodynamic particle size of 478.4 nm ± 90.87 and 322.8 ± 33.51, respectively. The mean particle size, zeta potential, and conductivity of materials also can be seen in Table 2.

Cytotoxicity of CAS–CH nanohybrid

Evaluation of cytotoxicity was determined with the help of the MTT assay and by visualizing morphological changes in the treated cells. The viability of RAW 264.7 cells as determined by MTT assay was found to decrease with an increase in concentration in all the test groups as compared with the control. The results showed a dose-dependent effect of the synthesized material extract on survivability of the cells at all milling cycles ($P < 0.05$). Survivability of cells were found to be 82%, 85%, and 92% at an exposure of X/4 concentration which decreased to 77%, 84%, and 86% at X/2 and 72%; 76% and 83% at X concentrations of CAS–CH 1H, CAS–CH 2H, and CAS–CH 3H, respectively. These reductions were statistically significant compared to the untreated cells used as control. Analysis of results clearly showed that the survivability of the cells was proportional to the milling time of the test material, where cells treated with CAS–CH 3H extract showed maximum viability, which decreased with a subsequent decrease in milling time ($P < 0.05$) (Fig. 4). Interestingly, the survivability of cells was comparatively much less in the case of CAS treated cells

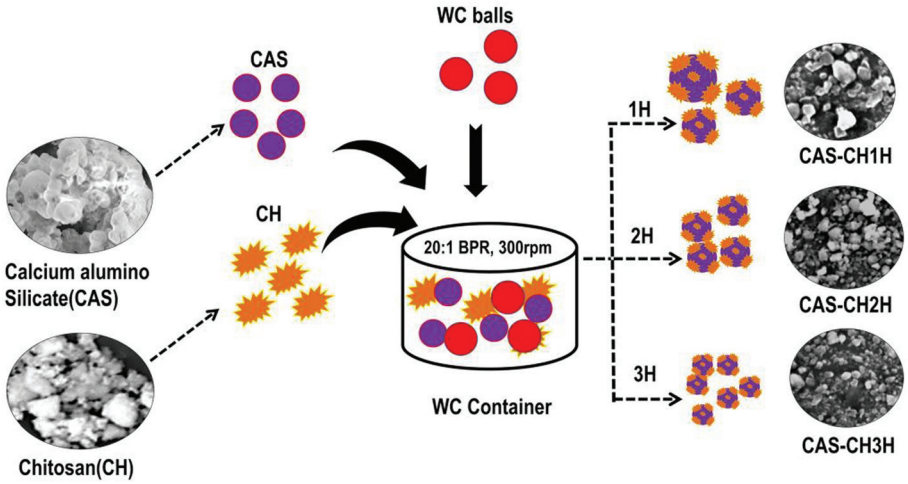

Fig. 1 Synthesis of CAS–CH by the high energy ball milling (HEBM) technique.

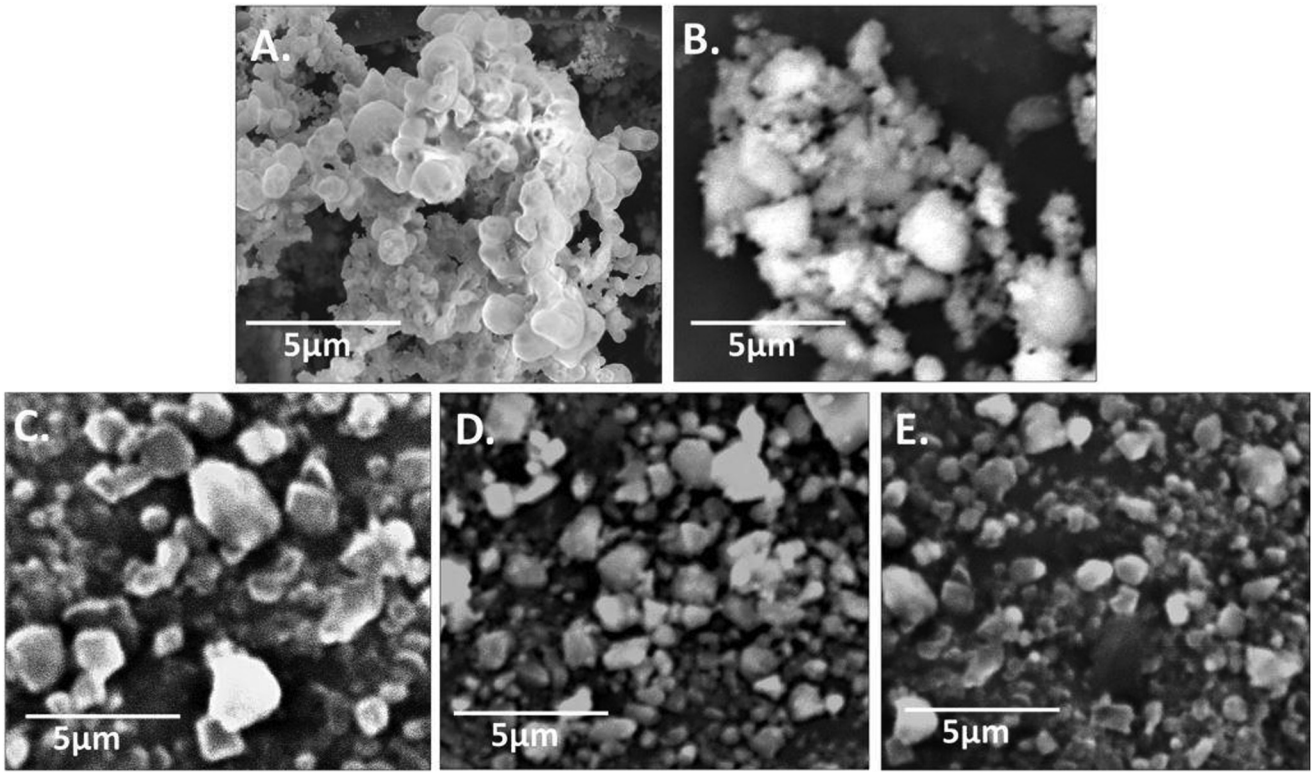

Fig. 2 Scanning electron micrographs of HEBM synthesized CAS, CH, and CAS–CH nanohybrid (A) CAS, (B) CH, (C) CAS–CH 1H, (D) CAS–CH 2H, and (E) CAS–CH 3H.

Table 1 Average particle size and particle size distribution of CAS–CH nanohybrids synthesized by HEBM at different milling times as determined by SEM analysis

Nanohybrid	Particle size distribution	Average particle size
CAS–CH 1H	2.8 nm–2100 nm	252 nm
CAS–CH 2H	2.8 nm–1400 nm	97.795 nm
CAS–CH 3H	2.8 nm–680 nm	58.825 nm

Table 2 Hydrodynamic size and zeta potential of CAS–CH nanohybrids synthesized by HEBM at different milling times as determined by dynamic light scattering

Nanohybrid	Hydrodynamic size	Zeta potential	Conductivity
CAS–CH 1H	576.7 ± 111.1 nm	−48.3 mV	0.137 mS cm^{-1}
CAS–CH 2H	478.4 ± 90.87 nm	−47.8 mV	0.134 mS cm^{-1}
CAS–CH 3H	322.8 ± 33.51 nm	−46.7 mV	0.104 mS cm^{-1}

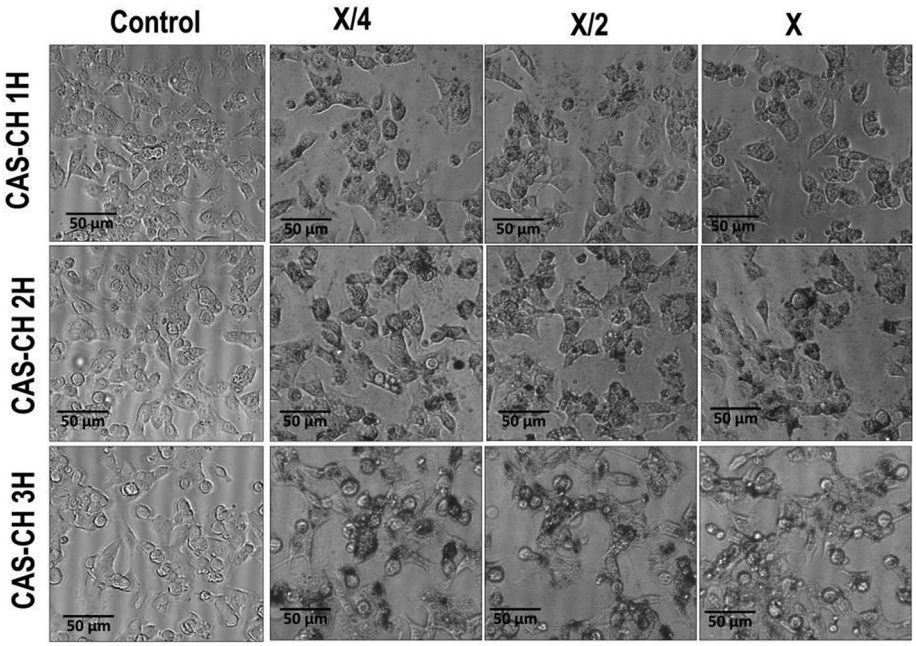

Fig. 3 Morphological changes in RAW264.7 cells exposed to HEBM synthesized CAS–CH nanohybrids.

while chitosan (CH) showed biocompatible behavior when used alone. As shown in Fig. 3, the morphology of the cells was found to be disorganized (loss of cellular attachment and blebbing), in case of CAS–CH 1H exposure and the degree of disorganization increased in severity with increase in concentration of material extracts ($P < 0.05$). Qualitatively, there was also a clear visualization of accumulated test material on the surface of cells. Interestingly, unattached cells without morphological changes were significantly fewer in number with the increase in milling time, showing a direct correlation of enhanced biocompatibility with increasing milling time.

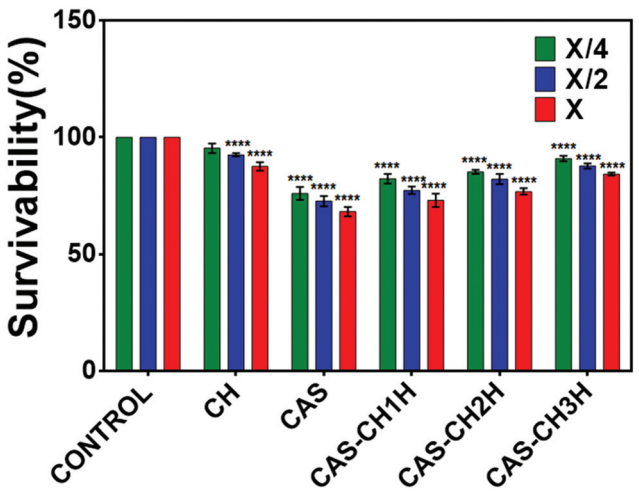

Fig. 4 Survivability of RAW 264.7 cells exposed to CAS–CH nanohybrid synthesized by HEBM at different milling times. All experiments were done in triplicate and data is presented as mean ± SD of three independent experiments. Statistical analysis was performed using GraphPad Prism v6.01 (San Diego, California). The data was subjected to two-way ANOVA with level of significance set at $P < 0.05$. Differences between groups were analyzed by Tukey's HSD test for multiple comparisons. *$P < 0.05$ denotes significant change from Bulk particles, number of * represents the degree of significance.

In order to compare the biocompatibility of CAS–CH synthesized at three time points, the survivability, cell morphology, attachment, and proliferation of RAW264.7 cells were checked with commonly used, commercially available Mineral Trioxide Aggregate (Pro Root MTA, Dentsply Sirona, USA) exposed at X, X/2, and X/4 concentrations. As shown in Fig. S1,† survivability of cells was found to be 55%, 68%, and 76% at X, X/2, and X/4 concentrations of exposed MTA which was significantly lower than the synthesized CAS–CH. ESI Fig. S2† shows the attachment and proliferation of cells in presence of MTA at different concentrations. As observed by morphological analysis, it was clearly found that cells lost their original morphology due to attachment of MTA at X/4 concentration. At higher concentrations of X/2 and X, there was detachment of cells from the surface as well as blebbing and morphological changes. Interestingly, the effects were more severe as compared to cells exposed with synthesized CAS–CH at similar concentrations (Fig. 3).

Further, to understand cytotoxic effects of CAS–CH extract at the cellular level, oxidative stress induction was analyzed by determining ROS production in CAS–CH exposed RAW cells. As shown in Fig. 5, fluorescence intensity of DHE was found to be higher with an increase in concentration of CAS–CH extracts at all milling time points (IH-3H) when compared with the control ($P < 0.05$). This shows a dose dependent effect (X > X/2 > X/4) of the test material in its ability to produce ROS in the treated cells. However, amount of ROS generation were

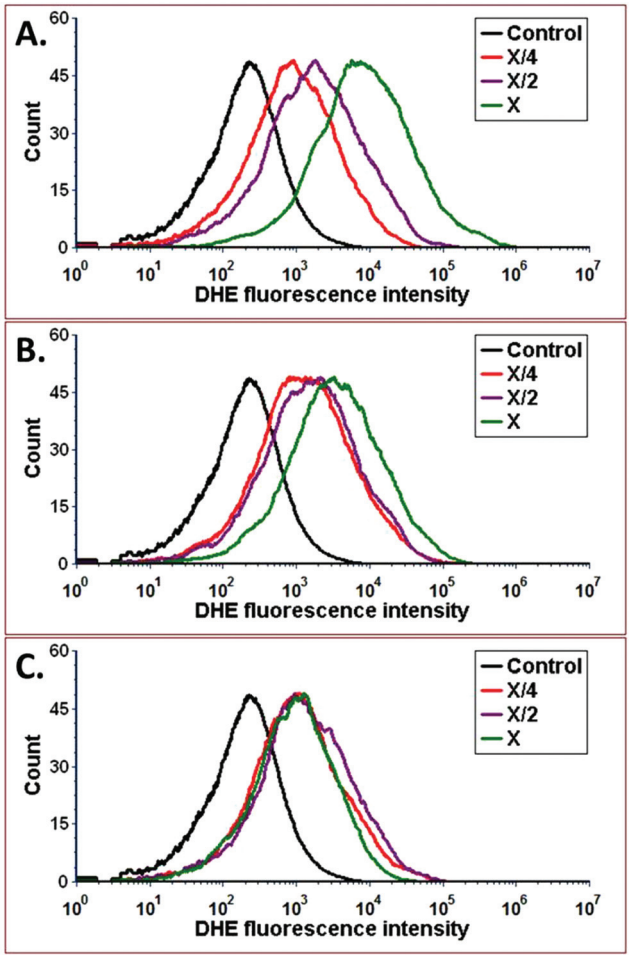

Fig. 5 ROS measurements of RAW264.7 cells treated with different concentrations of (A) CAS–CH 1H, (B) CAS–CH 2H, and (C) CAS–CH 3H nanohybrids synthesized by HEBM at different milling times. Treated cells were stained with DHE for the measurement of reactive oxygen species and analysed with the help of flow cytometry. The data was analysed with the help of FACS Express 6.0 (DeNovo, USA).

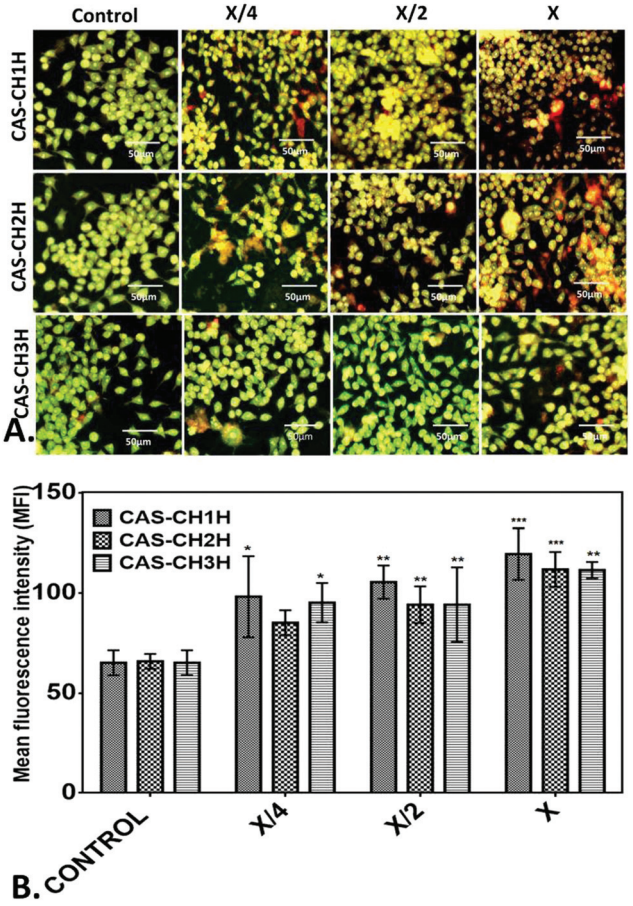

Fig. 6 Apotosis analysis of RAW 264.7 cells treated with different concentration of CAS–CH nanohybrid synthesized by HEBM at different milling times. The cells were stained with Acridine orange(AO)/EtBr after treatment with nanohybrids. (A) Fluorescent image of the stained cells. (B) Mean fluorescent intensity of the fluorescence of AO/EtBr stained cells. The images were analysed with help from Image J. All experiments were done in triplicate and data is presented as mean ± SD of three independent experiments. Statistical analyses were performed using GraphPad Prism v6.01 (San Diego, California). The data was subjected to two-way ANOVA with level of significance set at $P < 0.05$. Differences between groups were analyzed by Tukey's HSD test for multiple comparisons. *$P < 0.05$ denotes significant change from control and number of * represents the degree of significance.

reduced in the cells treated with extracts of material milled for longer durations (CAS–CH 3H). Determination of apoptosis as a consequence of oxidative stress was done by acridine orange – ethidium bromide staining which showed a highly significant difference in the mean fluorescence intensity of acridine orange (AO) within different dilutions of samples (X, X/2, X/4), $p < 0.001$ (Fig. 6). Similarly, a significant difference in the mean fluorescence intensity (MFI) of acridine orange was seen at different time points of milling ($p < 0.05$). Interestingly, the fluorescent intensity diminished with an increase in milling time of CAS–CH. Qualitatively, cells treated with CAS–CH 1H bulk (X) concentration extract showed late apoptosis. The cells in this group were stained orange (due to incorporation of ethidium) and showed condensed and fragmented nuclei. Apoptosis in early stage was seen in cells treated with CAS–CH 2H (X) and CAS–CH 1H (X/2). Cells in these groups were stained green with less uptake of ethidium bromide, showing chromatin condensation and nuclear fragmentation. Cells treated with CAS–CH 3H (X) showed early apoptotic changes; however, it was significantly less when compared to cells treated with extracts from lower milling times (1H and 2H). Cells treated with test group extracts showed higher apoptotic changes when compared with the control (untreated) and a concentration dependent result was observed in all the groups studied qualitatively. Overall, results showed a highly significant dose-dependent (X > X/2 > X/4) and milling time-dependent (1H > 2H > 3H) cytotoxic effect of material extracts on the exposed cells.

In silico investigation of CAS–CH nanohybrid interaction

To investigate cytotoxic effects of the CAS–CH nanohybrid at a molecular level, an *in silico* approach was taken using mole-

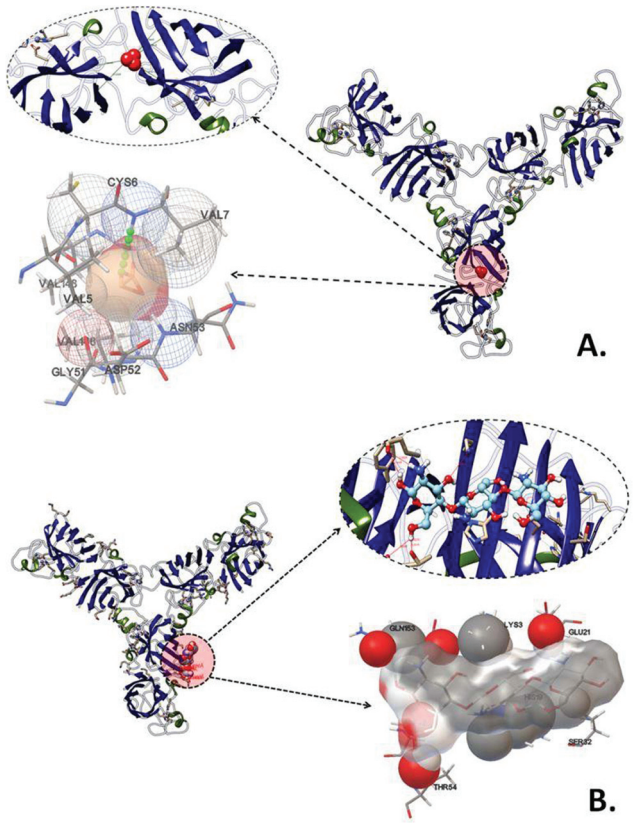

Fig. 7 Molecular docking analyses of interaction of Sod1 proteins with CAS and CH nanoparticles showing interacting amino residues (A) Sod1 with CAS and (B) Sod1 with CH.

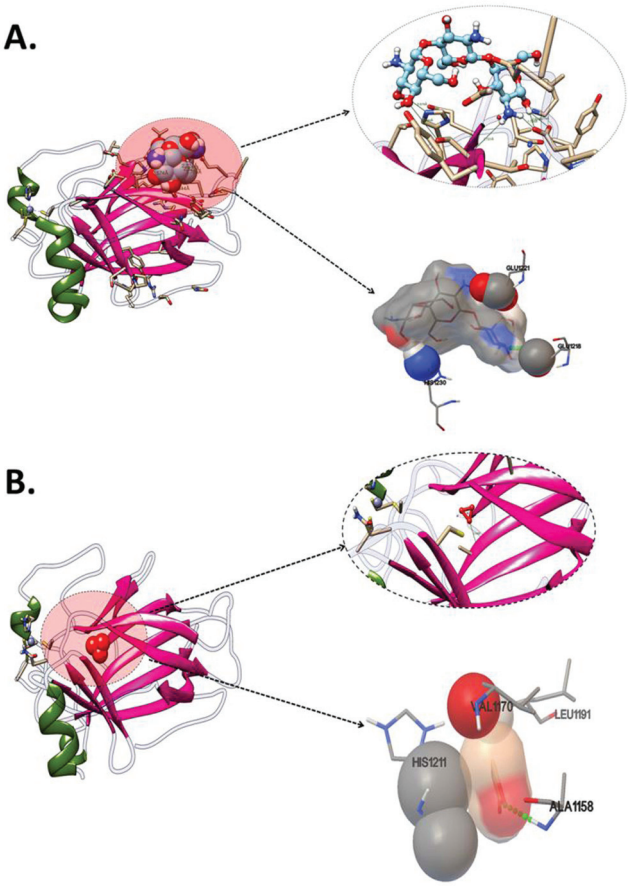

Fig. 8 Molecular docking analyses of interaction of P53 proteins with CAS and CH nanoparticles showing interacting amino residues (A) P53 with CH (B) P53 with CAS.

cular docking analysis of calcium aluminosilicate and chitosan with Sod1[24] as oxidative stress and p53[25] as apoptosis related proteins. As shown in Fig. 7, CAS was predicted to interact with Sod1 with Cys6 amino acid residue *via* hydrogen bond interaction with a binding energy of −4.8 kcal mol^{-1} (Fig. 8, Table 3). The other amino acids found to interact were Val5, Asn53, Gly51, and Asp52 *via* hydrophobic interactions. Chitosan (CH), the other part of the CAS–CH nanohybrid was found to interact with Sod1 *via* a hydrophobic interaction with Lys3, Gln153, Glu21, Ser32, and Thr54 amino acid residues (Fig. 6, Table 3). Autodock predicted interaction of CAS with p53, the apoptosis related protein, *via* Ala1158 through hydrogen bond interaction with a binding energy of −5.87 kcal mol^{-1}. The other amino acids involved in the interaction were Leu1191, Val1170, and His1211; however, their interactions were through hydrophobic means (Fig. 7, Table 3). The chitosan (CH) part of the nanohybrid was found to have a strong hydrogen bond interaction with p53 *via* a glu1218 residue. The other amino acid residues which were predicted to take part in the interaction were Glu1221 and His1230 through hydrophobic means. The total binding energy of CH was found to be −0.69 kcal mol^{-1} (Fig. 7, Table 3).

Discussion

This study elucidates the blending of chitosan with calcium aluminosilicate (CAS) to enhance biological properties of the later. A detailed depiction of the material's cytotoxicity was studied using macrophages treated with its extract. Calcium aluminosilicate with a 30–50% alumina in calcium phase compared to 5% alumina of Portland cement is a well-established material for orthopedic applications.[26] Properties like biogenic acid resistance, bioactivity, and durability make CAS a popular candidate to be evaluated as a potential dental bioceramic.[26,27] However, like other bioceramics, it also possesses a similar clinical deficiency of having a poor washout resistance when it comes in contact with tissue fluids and blood.[28] Other demerits include long setting times and reduced surface hardness and compressive strength in the surgical field.[29] Since, it is impossible to maintain a dry field during operative procedures, bioceramics show underutilization of their properties during clinical applications. Chitosan (CH), having osteogenic potential and antibacterial efficacy, has been previously investigated as a substitute for graft hemostasis.[30] Moreover, it offers an advantage as its hemostatic property is due to a poly-

Table 3 Binding energy and other parameters obtained by molecular docking analysis of interactions of different proteins with CAS–CH nanohybrids

Structure	Binding energy	Ligand efficiency	Inhibition constant	Intermolecular energy	Vander wall disolvation energy	Electrostatic energy	Total energy	Torsional energy
Sod1-chitosan	−2.16	−0.06	26.19	−7.53	−4.58	−2.68	−7.41	5.37
Sod1-calcium-alumino-silicate	−4.8	−0.96	304.26	−5.07	−5.07	0.1	0.1	0.27
P53-chitosan	−0.69	−0.02	309.69	−6.06	−2.54	−3.53	−5.91	5.37
P53-calcium aluminosilicate	−5.87	−1.17	49.71	−6.51	−6.51	0.1	0.1	0.27

cationic nature, which is independent of the coagulation cascade.[31]

With the need to improvise properties of CAS for dental applications, the present work describes a novel and industrial method of its blending with chitosan. This led to the formation of a CAS–CH nanohybrid having enhanced biocompatibility. Industrial synthesis was accomplished by well-known HEBM which has been reported previously to synthesize nanomaterials by gradual grinding, leading to reduction in particle sizes with increase in milling time.[32] HEBM has been well-recognized for green synthesis of nanomaterials and composites with a yield of bulk quantity and controlled size. CAS–CH synthesis was performed by milling at 1H, 2H, and 3H for proper blending and size reduction. To control size and avoid heating and aggregation of the material, milling time was maintained adequately and milling speed was maintained at 300 rpm. The synthesized CAS–CH nanohybrid collected at three time points of 1H, 2H, and 3H showed significant variability and reduction in their sizes with increase in milling time as determined by SEM and DLS. SEM analysis revealed concordance with previous literature showing a milling time-dependent decrease in particle size in TiO_2 nanoparticles.[18] Hydrodynamic size and zeta potential of CAS–CH was determined in cell culture medium in order to investigate their properties with respect to cellular physiological conditions. Hydrodynamic size of the material was found to decrease with an increase in milling time showing accordance with the results obtained from SEM. However, the larger size of particles as observed in DLS can be attributed to the presence of attached water and salt molecules present in the culture media.[33] To determine the ability of agglomeration of the material, its zeta potential was evaluated, which is the measure of the electrokinetic potential.[34] The zeta potential of a nanomaterial affects its surface ionization and dispersion stability. As shown in Table 2, there was a slight increase in the zeta potential with an increase in milling time. A probable explanation for this could be a change of shape and size of the nanoparticles with the blending of CAS with CH due to milling. The combined effect of CAS and CH lead to a change in net surface charge of material with a decrease in size.

Since the synthesized material had particles of variable sizes in the nanometer range, containing both inorganic (CAS) & organic (CH) structural units, it was categorized as a nanohybrid.[35]

It is important to test cytotoxicity of potential dental materials since they are supposed to be in intimate contact with a tooth and its surrounding tissues.[36] Cell cultures are the most widely used system to assess toxicity of materials.[37] They also provide a clearer perspective about a comprehensive understanding of *in vitro* cytotoxicity including parameters like cell morphology, attachment, proliferation, and viability.[38] Macrophages in a mammalian body have been reported to play a significant role in filtration and clearing of small particles.[39] They have been found to be involved in all stages of immune responses.[40] To perform their immunological response, macrophages have been reported to produce reactive oxygen species (ROS) and Nitric oxide (NO).[41,42] Hence, they can act as suitable sensors for analyzing potential cytotoxic effects of any foreign particles exposed to a mammalian body. With respect to these properties, the experimental material (CAS–CH) was assessed for its cytotoxicity against murine macrophages to assess its biocompatibility. The viability of the macrophages was found to decrease with increases in concentration from X/4 to X, whereas viability increased with exposure to extracts of the material milled for longer duration. This result indicated the concentration and milling time dependent cytotoxicity of synthesized nanohybrid in macrophages. The morphological analysis supported the results obtained in the viability assay, exhibiting a lesser number of damaged cells exposed to low concentrations of material extract. The cells were found to lose their original morphology and were detached from the surface at a higher concentration (X) as compared to X/2 and X/4. Similar interpretation was observed in case of CAS–CH 1H as compared to CAS–CH 2H and CAS–CH 3H. This toxic behavior at higher concentrations can be attributed to increased accumulation of nanohybrid material on the surfaces of macrophages leading to their internalization inside cells through endocytosis[43,44] as compared to exposure of low concentrations of the extract. Another important correlation for this result is the absence of equilibrium in the cell culture environment due to constant contact of cells with material extract. The extract was not eliminated in the current experimental setting, whereas under *in vivo* conditions, *peri*-apical innate defense and lymphatics tend to remove toxic substances due to constant flow of tissue fluids. It can thus be extrapolated that the concentration dependent toxic effects of materials *in vitro* are exacerbated when compared to their effects *in vivo*.[45]

Exhibition of lower toxicity at longer milling time points can be explained by the presence of blended chitosan with CAS which has been reported to be biocompatible at a specific concentration.[46] It can be deduced that CAS–CH 3H, 2H, and

1H exhibited comparative biocompatibility considering the biocompatibility of CH as a threshold parameter. Moreover, CAS alone was found to be cytotoxic in this comparison. The increase in milling time could have contributed to enhancing the blending of CH with CAS. The enhanced blending can be explained by a reduction in the toxic effects of CAS. Moreover, the cytotoxic effects were found to be less severe than with the commercially available dental material MTA at similar concentrations. Henceforth, with reference to the results it can be concluded that CH played a crucial role in enhancing the biocompatibility of CAS.

Literature is replete in showcasing mechanisms of toxicity exhibited by nanomaterials and hybrid materials. It has been reported that a decline in viability of cells can be caused by cessation of cell proliferation due to factors like change in cell redox potential[47] due to size and charge of exposed nanomaterial and induction of apoptosis followed by cellular necrosis.[48] However, a majority of reports have attributed the generation of oxidative stress for this phenomenon.[49] With reference to these previous reports, the mechanism of cytotoxicity possessed by CAS–CH can be ascribed to their charge, size, and generation of oxidative stress. Henceforth, to explore the mechanism of toxicity behavior of our CAS–CH nanohybrid, oxidative stress analysis and its consequent effect on apoptosis was analyzed using experimental and computational approaches. Experimental observations depicted a decrease in the induction of ROS with increase in milling time of the material. This again could be explained by the effect of increased blending of CAS and CH, contributing towards an enhancement in the biocompatibility of the material. ROS was found to be increased with increase in concentration of all three CAS–CH 1H, CAS–CH 2H, and CAS–CH 3H materials. This concentration dependent effect of material extract towards ROS production can be explained by rapid internalization of material molecules at high concentrations[50] and interaction of these materials with cytoplasmic contents, especially the mitochondrial respiratory chain. Previous reports have indicated similar interpretations in a case of metal nanoparticles.[51] Results obtained through experimental apoptosis analysis were in correlation with results obtained from oxidative stress analysis where the cells were found to be more apoptotic in CAS–CH 1H as compared to CAS–CH 2H and CAS–CH 3H at the same concentration. Moreover, induction of apoptosis was higher at higher concentration (X) as compared to lower concentrations (X/2, X/4) indicating the concentration and milling time dependent cytotoxicity of the CAS–CH nanohybrid. With reference to the oxidative stress and apoptosis experimental analysis results, it can be interpreted that the concentration dependent increase in the number of apoptotic cells due to exposure of CAS–CH is due to enhanced ROS induction by interaction of internalized molecules with cytoplasmic contents. The cytotoxic effect decreases with increase in milling time due to reduction of the CAS effect by CH.

Computational investigation predicted a molecular level interaction of CAS and CH with oxidative stress related protein Sod1 and apoptosis protein P53 through different amino acids *via* hydrophobic and hydrogen bond interactions. It can be reasoned that these interactions influence the structural configuration and functionality of Sod1 and P53, which leads to the abnormality in oxidative, stress induction, and induction of apoptosis. A similar explanation for cytotoxic effects of a HEBM synthesized nanomaterial like TiO_2 has been reported in recent literatures.[44]

Hence, considering results and interpretations obtained experimentally, computationally, and with reference to previously reported literature, the mechanism of the concentration dependent cytotoxicity of CAS–CH can be deduced as: upon exposure of cells with CAS–CH synthesized at 1H, 2H, and 3H, the molecules of the material becomes internalized inside the macrophages in a size dependent manner. The smaller the size, the higher is the uptake inside cells. The physiochemical properties of the material differ due to unequal composition of CAS and CH in the hybrid. Hence, the after effect of internalization of the molecules of each material varies accordingly. Following internalization, the molecules interact with cytoplasmic contents and organelles, interfering with their functional activity. Moreover, the CAS–CH molecule interacts with Sod1 and P53 enzymes influencing their functional activity. Due to these combined effects, there is a concentration dependent higher induction of ROS which further leads to induction of apoptosis in cells. Since the molecular

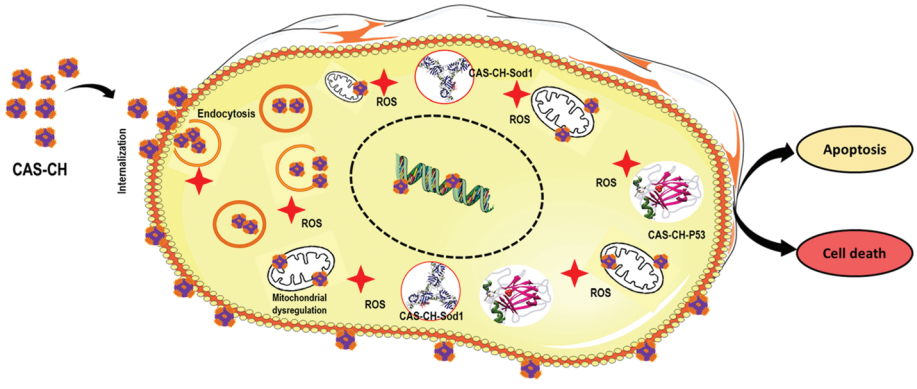

Fig. 9 Schematic presentation of mechanism of cytotoxicity of CAS–CH with macrophages.

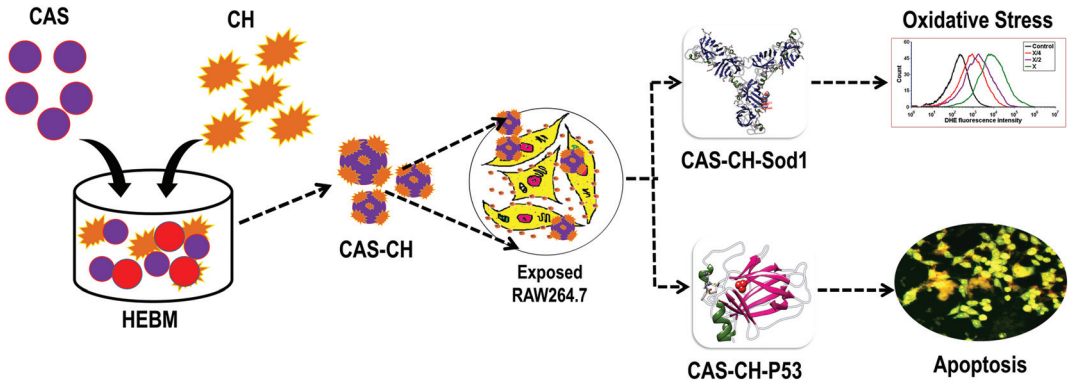

Fig. 10 Graphical summary of the work flow.

properties of the materials vary with milling time, the ROS generation and induction of apoptosis also varies accordingly. Thus, it can be concluded that the cytotoxicity of CAS molecules becomes varied due to blending of CH and this phenomenon is exhibited in a size and milling time dependent manner. This phenomenon can be understood pictographically as summarized in Fig. 9.

Conclusion

In brief, as shown in Fig. 10, the current study proposed a green synthesis of calcium aluminosilicate–chitosan (CAS–CH) nanohybrid for its potential dental application. A successful synthesis was carried out using the HEBM technique. Determination of physiochemical properties of synthesized nanohybrids showed alterations in size and zeta potential with milling time revealing the blending of CAS and CH. Cytotoxicity analysis of CAS–CH with RAW264.7 cells showed size and milling time dependent behavior. Cellular and molecular investigation revealed the mechanism of cytotoxicity as a consequence of the concentration dependent internalization of nanohybrids inside cells leading to their interaction with cellular proteins like Sod1 and p53. This interaction resulted in abnormal functionality of these proteins ensuing oxidative stress and apoptosis in the cells. The enhanced blending of chitosan as a result of an increase in milling time had a positive influence on biocompatibility of the nanohybrid. This study showed positive results for using chitosan with bioceramics like calcium aluminosilicate for an overall enhancement of its biocompatibility.

Conflicts of interest

There are no conflicts to declare.

Acknowledgements

The authors acknowledge Indian Association of Conservative Dentistry and Endodontics (IACDE) for funding the study through the IACDE Student's Research Grant. The authors thank Dr SKS Parashar for providing ball milling facility for the material synthesis.

References

1 Y. K. Mishra and R. Adelung, *Mater. Today*, 2017, DOI: 10.1016/j.mattod.2017.11.003.
2 H. D. L. Robert and B. Heimann, in *Bioceramic Coatings for Medical Implants*, Wiley-VCH Verlag GmbH & Co. KGaA, Weinheim, Germany, 2015, pp. 69–112.
3 O. Lupan, T. Braniste, M. Deng, L. Ghimpu, I. Paulowicz, Y. K. Mishra, L. Kienle, R. Adelung and I. Tiginyanu, *Sens. Actuators, B*, 2015, **221**, 544–555.
4 R. Morsy, R. Abuelkhair and T. Elnimr, *Silicon*, 2017, **9**, 489–493.
5 Y. K. Mishra, S. Kaps, A. Schuchardt, I. Paulowicz, X. Jin, D. Gedamu, S. Freitag, M. Claus, S. Wille, A. Kovalev, S. N. Gorb and R. Adelung, *Part. Part. Syst. Charact.*, 2013, **30**, 731–731.
6 M. Trope, A. L. F. Bunes and G. Debelian, *Endod. Top.*, 2015, 86–96.
7 K. Lin, W. Zhai, S. Ni, J. Chang, Y. Zeng and W. Qian, *Ceram. Int.*, 2005, **31**, 323–326.
8 H. H. Beheri, K. R. Mohamed and G. T. El-Bassyouni, *Mater. Des.*, 2013, **44**, 461–468.
9 M. Torabinejad and N. Chivian, *J. Endod.*, 1999, **25**, 197–205.
10 D. M. Escobar-García, E. Aguirre-López, V. Méndez-González and A. Pozos-Guillén, *Biomed. Res. Int.*, 2016, **2016**, 7926961.
11 M. Torabinejad and M. Parirokh, *J. Endod.*, 2010, **36**, 190–202.
12 M. Parirokh and M. Torabinejad, *J Endod*, 2010, **36**(1), 16–27.
13 G. G. Mori, L. M. Teixeira, D. Louzada de Oliveira, L. M. Jacomini and S. Rodrigues da Silva, *J. Endod.*, 2014, **40**, 1485–1488.
14 S.-H. Oh, S.-Y. Choi, Y.-K. Lee and K. N. Kim, *J. Biomed. Mater. Res.*, 2002, **62**, 593–599.

15 M. H. Nekoofar, K. Oloomi, M. S. Sheykhrezae, R. Tabor, D. F. Stone and P. M. H. Dummer, *Int. Endod. J.*, 2010, **43**, 849–858.
16 R. Jayakumar, M. Prabaharan, S. V. Nair and H. Tamura, *Biotechnol. Adv.*, 2010, **28**, 142–150.
17 K. V. Harish Prashanth and R. N. Tharanathan, *Trends Food Sci. Technol.*, 2007, **18**, 117–131.
18 S. K. Verma, E. Jha, P. K. Panda, M. Mukherjee, A. Thirumurugan, H. Makkar, B. Das, S. K. S. Parashar and M. Suar, *Toxicol. Res.*, 2018, **7**, 244–257.
19 S. K. Verma, E. Jha, P. K. Panda, J. K. Das, A. Thirumurugan, M. Suar and S. Parashar, *Nanomedicine*, 2017, **13**, 43–68.
20 S. Kasibhatla, *Cold Spring Harbor Protoc.*, 2006, **2006**, pdb.prot4493.
21 Y. Wang, J. Xiao, T. O. Suzek, J. Zhang, J. Wang, Z. Zhou, L. Han, K. Karapetyan, S. Dracheva, B. A. Shoemaker, E. Bolton, A. Gindulyte and S. H. Bryant, *Nucleic Acids Res.*, 2012, **40**, D400–D412.
22 E. C. Meng, E. F. Pettersen, G. S. Couch, C. C. Huang and T. E. Ferrin, *BMC Bioinf.*, 2006, **7**, 339.
23 O. Trott and A. Olson, *J. Comput. Chem.*, 2010, **31**, 455–461.
24 S. K. Verma, E. Jha, P. Kumar Panda, A. Mishra, A. Thirumurugan, B. Das, S. Parashar and M. Suar, *Toxicol. Sci.*, 2017, **161**(1), 125–138.
25 P. Kumari, P. K. Panda, E. Jha, K. Kumari, K. Nisha, M. A. Mallick and S. K. Verma, *Sci. Rep.*, 2017, **7**, 16284.
26 W. Wei, Y. Qi, S. Y. Nikonov, L. Niu, R. L. W. Messer, J. Mao, C. M. Primus, D. H. Pashley and F. R. Tay, *J. Endod.*, 2012, **38**, 936–942.
27 F. S. Shirazi, M. Mehrali, A. A. Oshkour, H. S. C. Metselaar, N. A. Kadri and N. A. Abu Osman, *J. Mech. Behav. Biomed. Mater.*, 2014, **30**, 168–175.
28 J. Camilleri and T. R. Pitt Ford, *Int. Endod. J.*, 2006, **39**, 747–754.
29 M. H. Nekoofar, D. F. Stone and P. M. H. Dummer, *Int. Endod. J.*, 2010, **43**, 782–791.
30 W. G. Malette, H. J. Quigley, R. D. Gaines, N. D. Johnson and W. G. Rainer, *Ann. Thorac. Surg.*, 1983, **36**, 55–58.
31 S. B. Rao and C. P. Sharma, *J. Biomed. Mater. Res.*, 1997, **34**, 21–28.
32 S. K. Verma, P. K. Panda, E. Jha, M. Suar and S. K. S. Parashar, *Sci. Rep.*, 2017, **7**(1), 13909.
33 J. Jiang, G. Oberdörster and P. Biswas, *J. Nanopart. Res.*, 2009, **11**, 77–89.
34 J. M. Berg, A. Romoser, N. Banerjee, R. Zebda and C. M. Sayes, *Nanotoxicology*, 2009, **3**, 276–283.
35 G. L. Drisko and C. Sanchez, *Eur. J. Inorg. Chem.*, 2012, **2012**, 5097–5105.
36 C. H. J. Hauman and R. M. Love, *Int. Endod. J.*, 2003, **36**, 75–85.
37 G. Schmalz, *J. Dent.*, 1994, **22**, S6–S11.
38 C. T. Hanks, J. C. Wataha and Z. Sun, *Dent. Mater.*, 1996, **12**, 186–193.
39 N. Fujiwara and K. Kobayashi, *Curr. Drug Targets: Inflammation Allergy*, 2005, **4**, 281–286.
40 X. Zhang and D. Mosser, *J. Pathol.*, 2008, 161–178.
41 M. Dorger and F. Krombach, *J. Aerosol Med.*, 2000, **13**, 369–380.
42 B. Fubini, *Ann. Occup. Hyg.*, 1998, **42**, 521–530.
43 L. Shang, K. Nienhaus and G. U. Nienhaus, *J. Nanobiotechnol.*, 2014, **12**, 5.
44 S. K. Verma, E. Jha, P. K. Panda, A. Thirumurugan, S. K. S. Parashar, S. Patro and M. Suar, *ACS Omega*, 2018, **3**, 1244–1262.
45 J. Camps and I. About, *J. Endod.*, 2003, **29**, 583–586.
46 I. Das, A. Padhi, S. Mukherjee, D. P. Dash, S. Kar and A. Sonawane, *Nanotechnology*, 2017, **28**, 165101.
47 A. Hoffman, L. M. Spetner and M. Burke, *J. Theor. Biol.*, 2001, **211**, 403–407.
48 E. Fröhlich, C. Samberger, T. Kueznik, M. Absenger, E. Roblegg, A. Zimmer and T. R. Pieber, *J. Toxicol. Sci.*, 2009, **34**, 363–375.
49 L. Yildirimer, N. T. K. Thanh, M. Loizidou and A. M. Seifalian, *Nano Today*, 2011, **6**, 585–607.
50 K. Donaldson, *Occup. Environ. Med.*, 2004, **61**, 727–728.
51 P. P. Fu, Q. Xia, H.-M. Hwang, P. C. Ray and H. Yu, *Nanomaterials*, 2014, **22**, 64–75.